Modified multi-scale constitutive model of Aluminum: complex loading with variable thermal conditions

A.A. Vshivkova, A.I. Shveykin, K.A. Romanov
Perm National Research Polytechnic University, Russia
vsivkovaa222@gmail.com, https://orcid.org/0009-0007-1365-9380
shveykin@pstu.ru, https://orcid.org/0000-0002-2656-0781
k.a.kriv@mail.ru, https://orcid.org/0000-0002-3599-7627

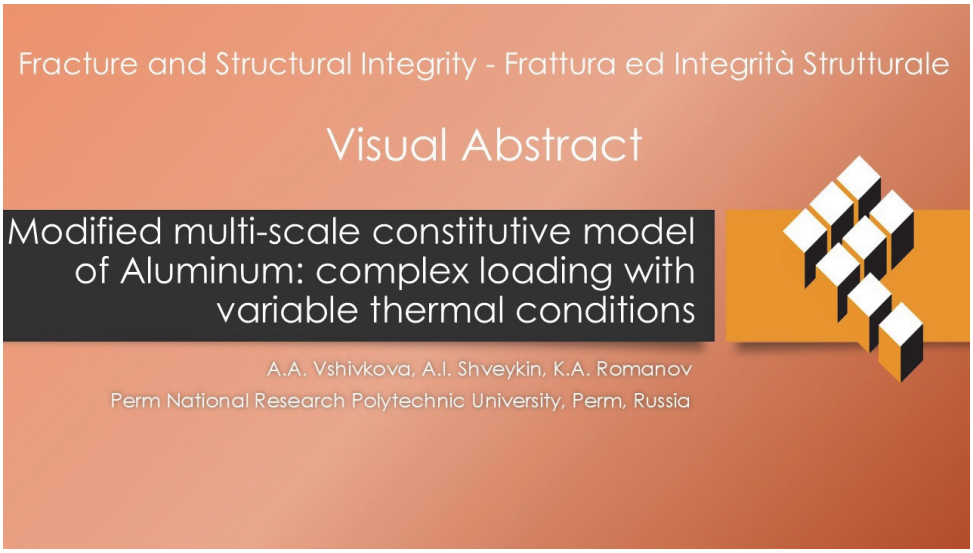

Citation: Vshivkova, A.A., Shveykin, A.I.., Romanov, K.A., Modified Multi-Scale Constitutive Model of Aluminum: Complex Loading with Variable Thermal Conditions, Fracture and Structural Integrity, 75 (2026) 351-361.

Received: 10.10.2025
Accepted: 10.11.2025
Published: 19.11.2025
Issue: 01.2026

KEYWORDS. Crystal plasticity, Statistical model, Complex and reverse loading, Temperature, Aluminum.

INTRODUCTION

At present, metal forming (MF) is applied to manufacture most products from metals and alloys, which entails shaping and/or surface treating such products to improve physical and mechanical properties [1].
The most well-known examples of such technological processes are rolling, forging, bulk and sheet stamping, extrusion, and drawing [1]. MF also includes processes of severe plastic deformation (SPD), which appeared at the end of the last century and has been actively developing in recent decades [2], e.g roller burnishing, multidirectional forging, rotary swaging, equal-channel angular pressing (ECAP), and others. SPD processes for large strains are associated with constraints, which make it possible to implement multipass processing (repetition of the same technological stage for several times). For example, during ECAP with a billet rotation between passes, the material is subjected to complex loading with a strain-path change [2]. In traditional MF processes, complex loading is often realized. For example, during deep drawing, at a certain

stage the deformation mode changes from pure shear to biaxial tension [3]. Experimental studies of complex loading and its effects are reported in many works, for example in [4].

During metal and alloy forming, in addition to complex loading, variations of temperature and/or strain rate in different parts of the billet are important [5]. Control of temperature and strain rate in these processes is necessary to achieve optimal conditions that ensure production of components with the best operational properties. To obtain such components, methods implementing dynamic recrystallization [6], phase transformations [7], and superplasticity modes [8] are applied. Examples of such MF methods include superplastic gas forming, superplastic rolling, hot stamping, forging, and rolling. Experimentally, the influence of temperature and strain rate variations on the material response has been studied in many works [6].

An exclusive use of experimental methods for studying MF processes is expensive and time-consuming; it results in increased material consumption and longer debugging times for new products. Therefore, the use of mathematical modeling methods to describe material behavior during MF processes, in addition to experimental studies, is an important task, especially now due to the growth of computational capabilities. Currently, a large number of macroscopic phenomenological models exist for the analysis of complex loading, as reported by many authors, e.g. [4, 9, 10]. Models of this class allow sufficiently accurate descriptions of complex and cyclic loadings but have certain limitations. In particular, they are applicable only to specific loading scenarios. When loading path changes, such model parameters must be redefined; it requires a large number of physical tests to identify parameters of the material constitutive model (CM) under different conditions. Furthermore, such models do not allow explicit descriptions of changes in the internal structure of the metal, which determine the final operational properties of the product. It should be noted that the evolution of microstructure (grain shape and size, texture, etc.) leads to various effects characteristic of complex and cyclic loadings: stress *dives* after path changes [3], cross-hardening [11], variations in the yield surface shape [10], and others.

Another class of constitutive models consists of multilevel CMs based on crystal plasticity [12]. The main difference between multi-level CMs and macroscopic phenomenological models is the evolution of the material internal structure and implementation of deformation mechanisms at different structural-scale levels. This is achieved by introducing internal variables and kinetic equations for their changes. These capabilities allow a single model with a fixed calibrated set of parameters to describe the material behavior under various conditions realized in MF technological processes. Furthermore, the model provides recommendations for the process improvement in terms of achieving enhanced operational characteristics.

In the present work, the application of previously tested two-level statistical CMs of FCC polycrystals [13, 14] is considered for a comprehensive description of aluminum behavior under complex loading with temperature variations. In the CM, the primary deformation mechanism is considered to be the intragranular slip of edge dislocations, and the rotation of crystallite lattices is taken into account. The relevance of studying the complex loading with temperature variations is determined by the presence of these factors in real technological processes of metal and alloy forming, e.g., rolling, stamping, forging, etc. A more detailed description of the model is provided in the following section of the paper. Next, presents the main results obtained under simple shear loading in both direct and reverse directions (reverse loading) with simultaneous temperature variations and under loading with a strain-path change, along with their discussion.

DESCRIPTION OF THE MATHEMATICAL MODEL

Previously, the authors have described the structure of multilevel models of inelastic deformation of metals and their alloys based on crystal plasticity [12]. Based on this structure, the authors proposed a constitutive model (CM) [14], modified by accounting for the combined influence of temperature and strain rate on the implementation of intragranular dislocation slips (IDS). When formulating the model [14], the conclusions of the analytical review [15] were used. The model includes two scale levels: macrolevel, i.e. the representative volume element (RVE) of the material, consisting of a large number of grains (crystallites) and mesolevel, i.e. the level of an individual grain. The model is statistical, and the relative arrangement of grains constituting the RVE is not considered. No separate scale level is introduced for subgrains. The model accounts for processes such as grain rotations (described using the Taylor constrained rotation model [16]), IDS, dislocation recovery and annihilation, and the resistance to dislocation slips from grain boundaries. It should be noted that there are crystal plasticity models based on the finite element method (CPFEM) that take into account the heterogeneity of deformations within a representative volume. Such models are more accurate than statistical ones, but are more computationally intensive. Therefore, with the focus on using constitutive models to describe the manufacturing and processing of large-sized products, the authors consider statistical models based on the Taylor hypothesis. At the same time, it is important to emphasize that the mesolevel equations discussed below can also be transferred to a CPFEM model.

In the equations below, *related* variables at different levels (stress measures, etc.) are denoted by the same letters: lowercase for the mesolevel, uppercase for the macrolevel. Macrolevel stresses are determined by averaging the stresses of the crystallites (hereafter the crystallite index is omitted): $\mathbf{K} = \langle \boldsymbol{\varkappa} \rangle$, where $\mathbf{K}$ is the weighted Kirchhoff stress tensor at the macrolevel, $\boldsymbol{\varkappa} = \overset{\circ}{\rho} / \hat{\rho} \boldsymbol{\sigma}$ is weighted Kirchhoff stress tensor at the mesolevel, $\boldsymbol{\sigma}$ is the Cauchy stress tensor at the mesolevel, $\overset{\circ}{\rho}$, $\hat{\rho}$ denote material density of the crystallite in the initial (unloaded) and current configurations, respectively, and, $\langle \cdot \rangle$ denotes the averaging operation. It should be noted that mesolevel relations can also be applied to direct models considering heterogeneous fields at the mesolevel.

The system of equations for each mesolevel element is given as [12]:

$$\begin{cases} \boldsymbol{\varkappa}^{cor} \equiv \dot{\boldsymbol{\varkappa}} - \boldsymbol{\omega} \cdot \boldsymbol{\varkappa} + \boldsymbol{\varkappa} \cdot \boldsymbol{\omega} = \overline{\mathbf{n}}_{(cor)} : \left(\mathbf{l} - \boldsymbol{\omega} - \mathbf{z}^{in} \right) \\ \mathbf{l} = \mathbf{L} \\ \mathbf{z}^{in} = \sum_{j=1}^{K} \dot{\gamma}^{(j)} \mathbf{b}^{(j)} \mathbf{n}^{(j)} \\ \dot{\gamma}^{(k)} = \dot{\gamma}_0 (\tau^{(k)} / \tau_c^{(k)})^{1/m} H\left(\tau^{(k)} - \tau_c^{(k)} \right), k = 1, ..., K \\ \tau^{(k)} = \boldsymbol{\varkappa} : \mathbf{b}^{(k)} \mathbf{n}^{(k)}, k = 1, ..., K \\ \boldsymbol{\omega} = \frac{1}{2} (\mathbf{l} - \mathbf{l}^{\mathrm{T}}) - \frac{1}{2} \sum_{k=1}^{K} \dot{\gamma}^{(k)} (\mathbf{b}^{(k)} \mathbf{n}^{(k)} - \mathbf{n}^{(k)} \mathbf{b}^{(k)}) \\ \dot{\mathbf{o}} \cdot \mathbf{o}^{\mathrm{T}} = \boldsymbol{\omega} \\ \boldsymbol{\varkappa}\big|_{t=0} = \boldsymbol{\varkappa}_0, \tau_c^{(k)}\big|_{t=0} = \tau_{c0}^{(k)}, \gamma^{(k)}\big|_{t=0} = \gamma_0^{(k)}, k = 1, ..., K, \mathbf{o}\big|_{t=0} = \mathbf{o}_0 \end{cases} \tag{1}$$

where $\boldsymbol{\varkappa}^{cor}$ is the corotational derivative of the mesolevel Kirchhoff stress tensor; $\boldsymbol{\omega}$ is the spin of a rigid moving coordinate system; $\overline{\mathbf{n}}_{(cor)}$ is the elastic stiffness tensor of the crystallite (which components are constant in the moving coordinate system); $\mathbf{l} \equiv \hat{\nabla} \mathbf{v}^{\mathrm{T}} = \dot{\mathbf{f}} \cdot \mathbf{f}^{-1}$ is the transpose velocity gradient; $\mathbf{f}$ is the deformation gradient in the initial configuration; $\mathbf{z} = \hat{\nabla} \mathbf{v}^{\mathrm{T}} - \boldsymbol{\omega}$ is the strain rate tensor; $\mathbf{z}^{in}$ is an inelastic part of the transpose velocity gradient; $\mathbf{b}^{(k)}$, $\mathbf{n}^{(k)}$, $\dot{\gamma}^{(k)}$, $\tau^{(k)}$, $\tau_c^{(k)}$ are the unit vectors of slip direction and slip plane normal, shear rate, shear stresses and critical resolved shear stresses for the k-th slip system (SS), correspondently; K is the number of slip systems of edge dislocations; $\mathbf{o}$ is the orthogonal tensor that determines the orientation of the crystallite's lattice (it connects the basis vectors of the moving coordinate system to the basis vectors of the fixed laboratory coordinate system); $\boldsymbol{\varkappa}_0$, $\tau_{c0}^{(k)}$, $\gamma_0^{(k)}$, $\mathbf{o}_0$ are initial values of stress tensor, critical shear stress, accumulated slip, orientation of the moving coordinate system, respectively; $\dot{\gamma}_0$, m are the model parameters; $H(\cdot)$ is the Heaviside function. Within this model, it is assumed that $\dot{\gamma}_0 = d_{int}$, where $d_{int} = \sqrt{(\mathbf{l}_{dev} - \boldsymbol{\omega}) : (\mathbf{l}_{dev} - \boldsymbol{\omega})^{\mathrm{T}}}$ is the intensity of deviator of the strain rate tensor [17], where $\mathbf{l}_{dev} = \mathbf{l} - sp(\mathbf{l})\mathbf{I}/3$, $sp(\mathbf{l})$ is the trace of tensor $\mathbf{l}$, $\mathbf{I}$ is identity tensor; $\mathbf{D} = \left(\mathbf{L} + \mathbf{L}^{T} \right) / 2$ is the symmetric part of the transpose velocity gradient. The mesoscale relations in the rate formulation (1) include [12]: the elastic law in rate form, the relation for specifying kinematic influences (for the statistical model, the Taylor hypothesis is used), the determination of the inelastic deformations rate through the shear rates along slip systems, the Hutchinson equation for their finding, the assignment of shear stresses on slip systems, the determination of the lattice spin (i.e. the spin associated with the elastic component of the vorticity tensor [16]) and the relationship of the orientation tensor connection with it, as well as the initial conditions for the model variables.

The equation for determining the critical shear stress per SS:

$$\tau_c^{(k)} = \tau_{dis}^{(k)} \left(\dot{\gamma}^{(i)}, \tau_c^{(i)}, T, d_{int} \right) + \tau_{lattice}^{(k)} \left(T, d_{int} \right) + \tau_b^{(k)}(T), \; i = 1, ..., K, \; k = 1, ..., K, \tag{2}$$

assumes the action of several softening and hardening mechanisms: $\tau_{dis}^{(k)}$ describes resistance to the dislocation slip from forest and other dislocation barriers, $\tau_{lattice}^{(k)}$ is a part associated with crystal lattice resistance, $\tau_{b}^{(k)}$ is a part associated with grain boundaries; T is the current temperature. Relations from [14] were used for all terms except $\tau_{dis}^{(k)}$ (modified as described below).

To find the *lattice* part the following equation is used [14, 18]:

$$\tau_{lattice}^{(k)} = \tau_0 \left(1 - A^{(k)} T \ln\left(\dot{\gamma}_{p0} / d_{\text{int}}\right)\right)^2 \tag{3}$$

where τ_0 is lattice resistance at 0 K, while $\dot{\gamma}_{p0}$, $A^{(k)}$ are model parameters.

The part associated with grain boundaries to hardening is described by the Hall–Petch law [18]:

$$\tau_{b}^{(k)}(T) = k_{HP}(T) d^{-0.5} \tag{4}$$

where $k_{HP}(T)$ is Hall–Petch coefficient, d is the mean grain size.

The component characterizing the barrier effect of the dislocation structure is described by:

$$\dot{\tau}_{dis}^{(k)} = \dot{\tau}_{hard}^{(k)}\left(\dot{\gamma}^{(m)}, T, d_{int}\right) - \dot{\tau}_{recovery}^{(k)}\left(\tau_c^{(k)}, T, d_{int}\right) H(\tau_{dis}^{(k)} - \tau_{dis\ threshold}^{(k)}) + \dot{\tau}_{reversal}^{(k)}$$

$$\dot{\tau}_{hard}^{(k)} = \sum_{l=1}^{\mathrm{K}} h^{(kl)}\ \dot{\gamma}^{(l)}$$

$$h^{(kl)} = \left[q_{\text{lat}} + (1 - q_{\text{lat}})\delta^{(kl)}\right] h^{(l)}, \quad h^{(l)} = h_0 \left(1 - \frac{\tau_c^{(l)}}{\tau_{sat} - f_2(T - T_{ref})}\right)^a \tag{5}$$

$$h_0 = h_{fixD} - f\left(T - T_{ref}\right)$$

$$\dot{\tau}_{recovery}^{(k)} = \tau_{dis}^{(k)} \left[\frac{a_2}{a_1 - a_2 T}\dot{T} + s\dot{\gamma}^{(k)}\right] \left(T - T_{ref}\right) \ln\left(\frac{\dot{\varepsilon}_0}{d_{int}}\right) H(T - T_{ref}) H(\dot{\varepsilon}_0 - d_{int})$$

In (5), in addition to previously introduced symbols: $\dot{\tau}_{hard}^{(k)}$ and $\dot{\tau}_{recovery}^{(k)}$ are components of strengthening due to dislocation interactions and softening due to diffusion processes; $\dot{\tau}_{reversal}^{(k)}$ considers effects related to dislocation annihilation under reverse loading; $\tau_{dis\ threshold}^{(k)}$ is the threshold value of the dislocation component of critical stresses (determined by the initial dislocation density), above which softening due to dislocation interactions and diffusion cannot be neglected; $h^{(kl)}$ is matrix characterizing interactions between different slip systems; q_{lat} is latent hardening coefficient (1.4 for non-coplanar, 1 for coplanar slip systems [19]); $\delta^{(kl)}$ Kronecker delta; τ_{sat} is saturation stress determined during model identification; a, f, f_2, h_{fixD}, a_1, a_2, s are model parameters; parameter $\dot{\varepsilon}_0$ characterizes strain rate above which diffusion processes become ineffective and T_{ref} characterizes temperature below which diffusion processes is ineffective too.

To extend the CM [14] for reverse loading, corresponding physical effects are included by adding term $\dot{\tau}_{reversal}^{(k)}$ to (5). During loading reversal, a so-called plateau forms in the stress-strain curve [9, 20], the length of which depends on temperature. Most researchers note that the plateau formation is primarily due to the loading reversal on the dislocation generation and

annihilation rates: a rapid annihilation of part of the substructures occurs, and the main dislocation sources (loops), which have not sufficiently expanded by the moment of direction change, start to collapse.

Several dislocation-oriented models account for these processes. In [20], a reverse component is distinguished in the total dislocation density, gradually annihilating after strain-path changes on SS. A similar separation is proposed in more complex models [21] considering parts associated with forest dislocations from different SS to hardening across all slip systems. Unfortunately, by introducing additional variables and evolution equations we will increase computational time, reduce applicability for real technological processes. Therefore, in this work, a simplified approach similar to [14] is used, and the effect of loading path-change is accounted for directly in the critical stress relation. It is assumed that the dislocation component $\tau_{dis}^{(k)}$ is fully determined by the evolution of dislocation densities.

Equations from [22] are used analogously. In [22], it is considered that dislocations blocked by various obstacles during *direct* motion gradually un-block during reverse loading (initially slowly, then rapidly, then gradually decreasing). This process is more intense at high temperatures. The reversal condition can be written as $\left(\gamma^{(2k)}-\gamma^{(2k+1)}\right)\left(\dot{\gamma}^{(2k)}-\dot{\gamma}^{(2k+1)}\right)<0$ (using a doubled set of SS, $2k$ and $2k+1$, i.e. numbers of *positive* and *negative* opposite SS, respectively), and the corresponding term in the hardening law has the following form:

$$\dot{\tau}_{reversal}^{(k)}=\begin{cases}-\dfrac{g\left(T-T_{ref}\right)}{\gamma_{new}^{(k)}\sigma_{\mathrm{R}}\sqrt{2\pi}}\exp\left(\dfrac{-\left(\ln\left(\left|\gamma_{new}^{(k)}\right|\right)-\mu_{\mathrm{R}}\right)^2}{2\sigma_{\mathrm{R}}^2}\right),\gamma_{new}^{(k)}>0\\ 0,\gamma_{new}^{(k)}\le 0\end{cases} \tag{6}$$

where $\gamma_{new}^{(k)}$ is slip on SS after the start of reverse loading; μ_{R}, σ_{R}, g are model parameters.

For initial conditions, it is assumed that the Hall–Petch coefficient and the initial dislocation structure resistance depend linearly on temperature [18, 23]:

$$\tau_c^{(k)}\Big|_{t=0}=\tau_{dis}^{(k)}\Big|_{t=0}+\tau_b^{(k)}\Big|_{t=0}+\tau_{lattice}^{(k)}\Big|_{t=0}=\alpha-\beta T\Big|_{t=0}+\tau_{lattice}^{(k)}\Big|_{t=0} \tag{7}$$

It is assumed in (7) that the initial dislocation structure is close to the natural configuration (dislocation density relatively low, no complex barrier structure). Modeling pre-deformed materials with a complex structure, including non-equivalence of the dislocation slip resistance in direct and reverse directions, requires a corresponding complication of relation (7).

RESULTS AND DISCUSSIONS

Direct loading

The model was applied to study the behavior of a representative volume of aluminum polycrystal consisting of 343 crystallites under simple shear conditions at various parameters. The initial orientation distribution was assumed to be uniform. Note that complex loading requires a larger representative volume (number of grains in the sample) than monotonic loading, but for uniform orientation distribution a sample size of 343 is quite sufficient; in calculations, the relative deviation of the results with an increase in sample size does not exceed 1 percent.

The model parameters m, Π_{1111}, Π_{1122}, Π_{1212}, $\dot{\gamma}_{p0}$, $\dot{\varepsilon}_0$ were taken as known ones and corresponded to the data reported in [17, 18, 23]. Based on the data about initial yield stresses at different temperatures, parameters $A^{(k)}$, α, β, τ_0 were determined. Parameters describing the response at low temperatures (h_{fixD}, τ_{sat} and a) were determined from loading diagrams at temperature (T) $T_{ref}=153\ K$. Subsequently, from the loading diagram at 293 K, the values of parameters f, f_2, s were obtained. A comparison of the calculated (model) and experimentally obtained data is shown in Fig. 1 below. In this case, the relative deviation of the numerical solution from the experimental data is less than 2.9%, where deviation defined as:

$$\max_{\varepsilon_i}\left|\frac{\sigma_{simulated}\left(\varepsilon_i\right)-\sigma_{experimental}\left(\varepsilon_i\right)}{\sigma_{experimental}\left(\varepsilon_i\right)}\right| \tag{8}$$

where ε_i are the strain intensities for which the flow stress is determined experimentally, $\varepsilon = \sqrt{2/3\,\boldsymbol{\varepsilon}(t):\boldsymbol{\varepsilon}(t)}$, where $\boldsymbol{\varepsilon}(t) = \left(\int_0^t \left(\frac{\mathbf{L}(\zeta) + \mathbf{L}^T(\zeta)}{2} \right) d\zeta \right)$ is strain tensor.

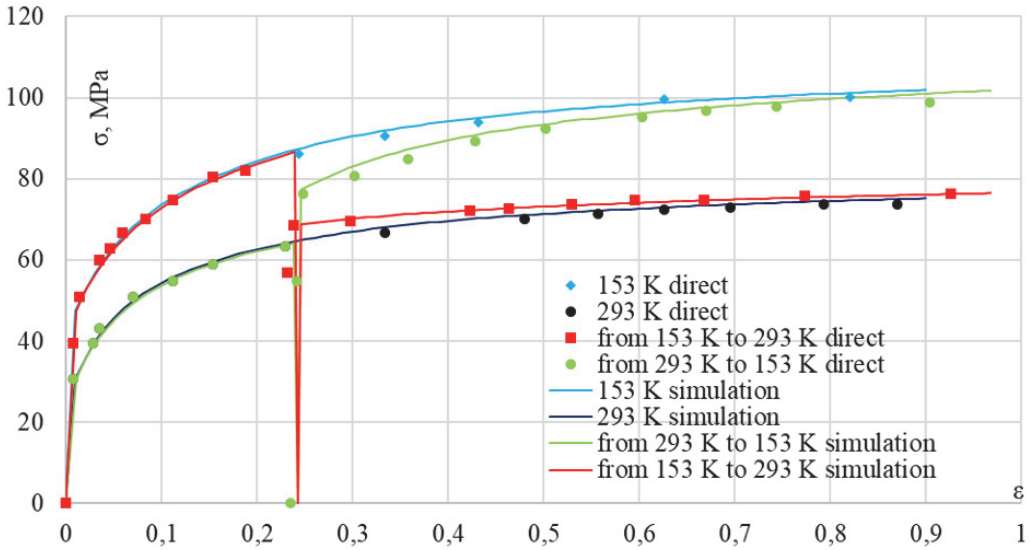

Figure 1: Dependence of shear stress on the shear component of strain tensor obtained in model calculations, along with experimental data [9] for aluminum under simple shear at a strain rate of 10^{-3} s^{-1} at various temperatures (T).

The parameters of the model identified for pure aluminum are presented in Tab. 1 below.

Parameter	Value	Parameter	Value
m	0.1	τ_0	23.645 MPa
h_{fixD}	0.34 GPa	$\dot{\gamma}_{p0}$	10^8 s^{-1}
a	2.6	$A^{(k)}$	$8.18 \cdot 10^{-5}$ K^{-1}
f	0.309 MPa/K	α	17.85 MPa
f_2	0.134 MPa·K	β	$2.42 \cdot 10^{-2}$ MPa/K
a_1	29.85 GPa	τ_{sat}	68 MPa
a_2	0.015 GPa/K	Π_{1111}	106.8 GPa
s	$9 \cdot 10^{-5}$ K^{-1}	Π_{1212}	28.3 GPa
$\dot{\varepsilon}_0$	10^8 s^{-1}	Π_{1122}	60.4 GPa
T_{ref}	153 K		

Table 1: Parameters of the constitutive model for aluminum.

The model described above makes it possible to sufficiently study deformation mechanisms and structural changes taking place in the material. In particular, the model allows assessment of various slip systems in the crystallites. In Fig. 2(a) and Fig. 2(b) below, data are presented on the number of crystallites in the representative volume, in which a certain number of slip systems are active (i.e., the Schmid criterion $\left|\tau^{(k)}\right| \geq \left|\tau_c^{(k)}\right|$ is satisfied) or near-active (with a tolerance of 5 MPa, i.e., in case $\left|\tau^{(k)}\right| \geq \left|\tau_c^{(k)}\right| - 5\,\text{MPa}$) under simple shear depending on the accumulated strain.

After analyzing the data in Fig. 2(b), it can be noted that at the initial stage of loading, the number of crystallites with a large number of near-active slip systems is high, which indicates that the stresses are located near the vertices of the yield surface of the crystallite [24]; similar results were obtained in [13, 25]. At the same time, the fraction of crystallites with 8 near-active

slip systems gradually decreases, while the number of crystallites with 6 near-active slip systems increases, which is consistent with the results of [25]. These tendencies can be explained by the fact that due to latent hardening, the yield surface is transformed – the 8th-order vertices [24] cease to exist. Moreover, as a result of rotations of the crystal lattice in different crystallites, the mesostress in the stress space moves between the transformed vertices along the faces and edges of the crystallite yield surface [13].

It should be noted that the diagrams evaluating the number of near-active slip systems more clearly reveal these transitional processes (Fig. 2(b)) than the diagrams for strictly active slip systems (Fig. 2(a)).

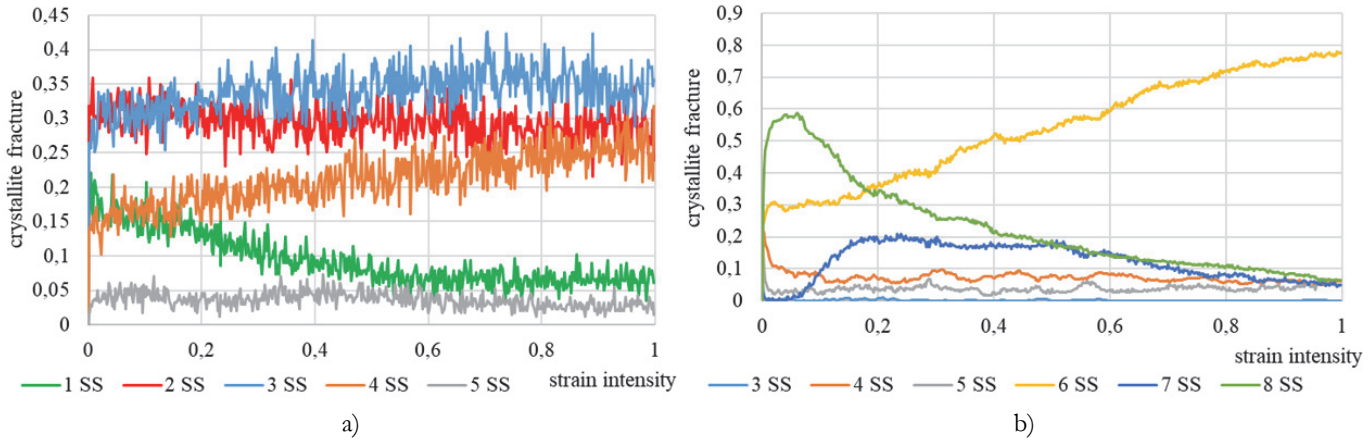

a) b)

Figure 2: Dependence of the fraction of crystallites with a certain number of (a) active and (b) near-active slip systems (SS) on the intensity of accumulated strain under simple shear of aluminum at a temperature of 293 K.

Reverse loading

Reverse loading of aluminum under shear at various temperature conditions was also simulated using the model described above. The results of numerical experiments and the corresponding experimental data [9] are shown in Fig. 3 below. The relative deviation of the numerical solution from the experimental data (8) is less than 7%.

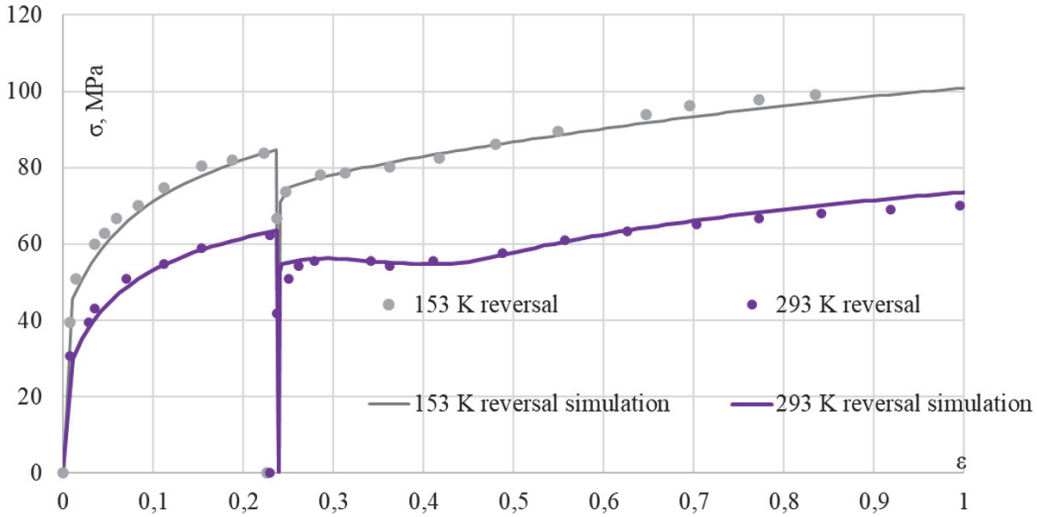

Figure 3: Dependence of shear stress on the shear component of the strain tensor obtained in model calculations, and experimental data [9] for reverse shear of aluminum at various temperatures

Analyzing the data in Fig. 4(a) and Fig. 4(b) on the slip system under reverse loading, it can be seen that after variations in loading directions, the fraction of crystallites with a smaller number of near-active slip systems (4 and 5) sharply increases. This may be associated with the fact that during the prestrain a significant number of dislocations accumulated at barriers for certain slip systems, and these slip systems are much more easily activated in the reverse direction compared to others.

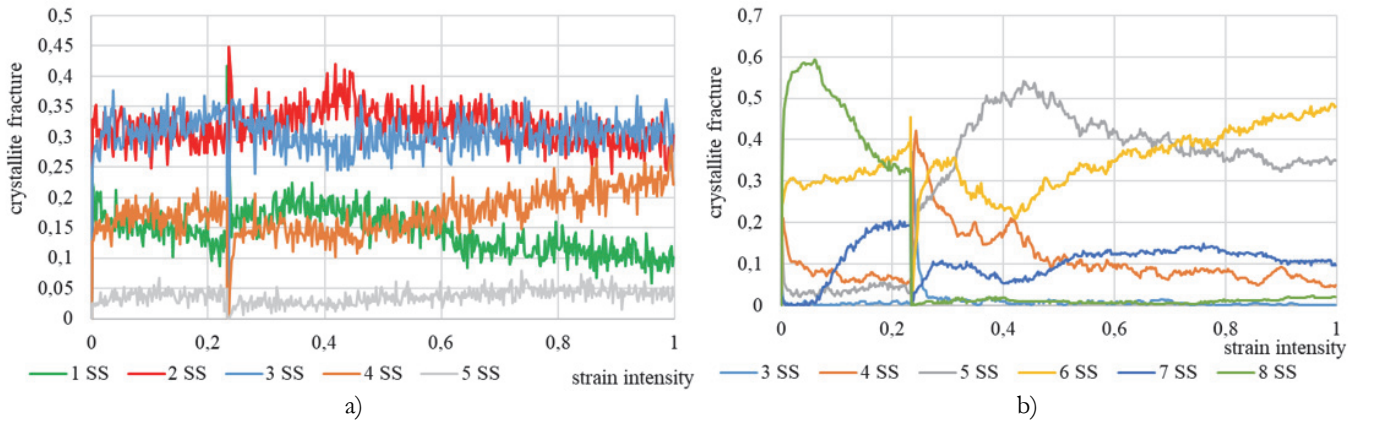

Figure 4: Dependence of the fraction of crystallites with a certain number of (a) active and (b) near-active slip systems on the intensity of accumulated strain under reverse shear of aluminum at a temperature of 293 K. The change in loading direction occurs at t=233 s.

Loading with strain-path change

Loading with a strain-path change, so-called orthogonal loading was simulated: up to t=233 s, quasi-uniaxial tension $\mathbf{L}=\dot{\varepsilon}\left[\mathbf{k}_3\mathbf{k}_3-0.5\left(\mathbf{k}_1\mathbf{k}_1+\mathbf{k}_2\mathbf{k}_2\right)\right]$ was applied; subsequently, unloading occurred and simple shear $\mathbf{L}=\dot{\varepsilon}\mathbf{k}_1\mathbf{k}_2$ was realized at the same strain rate, at a temperature of 293 K.

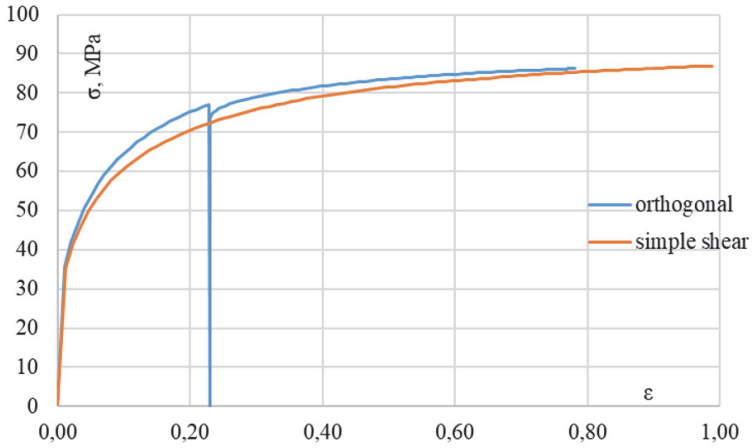

Figure 5: Dependence of stress intensity on the intensity of accumulated strain obtained in model calculations.

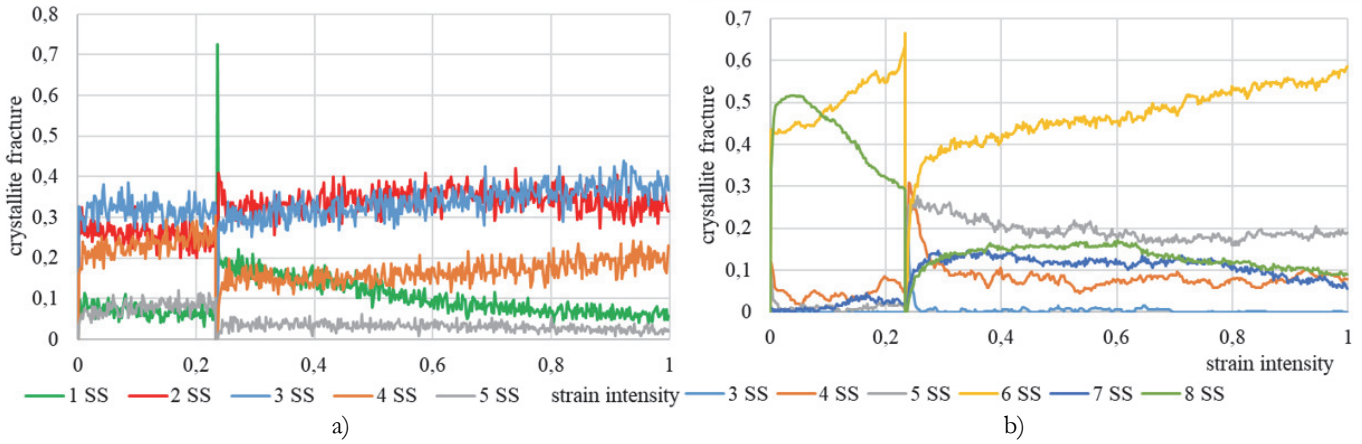

Figure 6: Dependence of the number of crystallites with a certain number of (a) active and (b) near-active slip systems on the intensity of accumulated strain under orthogonal loading of aluminum at a temperature of 293 K. The loading change occurs at t=233 s.

The diagrams shown in Fig. 5 qualitatively correspond to the data reported for alloy A5052-O in [11].
It should be noted that at the moment of the strain-path change, the number of slip systems with 6 and 8 near-active slip systems sharply decreases, while the number of crystallites with 4, 5, and 7 near-active slip systems increases (Fig. 6(b)). At the same time, the fraction of crystallites with 8 near-active slip systems under complex loading immediately after the strain-path change is noticeably lower than at the same accumulated strain under simple shear. This can be explained by latent hardening of the slip systems activated under shear but not active during the preliminary tension, which transforms the yield surface.

Loading with simultaneous strain-path change and temperature variations

Finally, the behavior of the representative volume was studied under conditions in which, simultaneously with the strain-path change (analogous to the case in the previous paragraph), the temperature varied: either a rapid cooling from 293 K to 153 K occurred (Fig. 7), or, conversely, a rapid heating from 153 K to 293 K took place (Fig. 8).

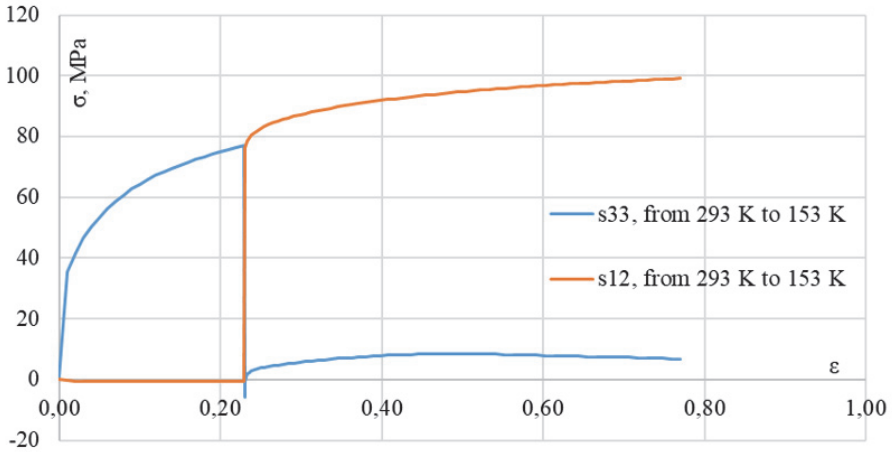

Figure 7: Dependence of stress components on the intensity of accumulated strain obtained in model calculations during rapid cooling from 293 K to 153 K. The legend uses the following notations: s33 is component of stress tensor σ_{33}, s12 is component of stress tensor σ_{12}.

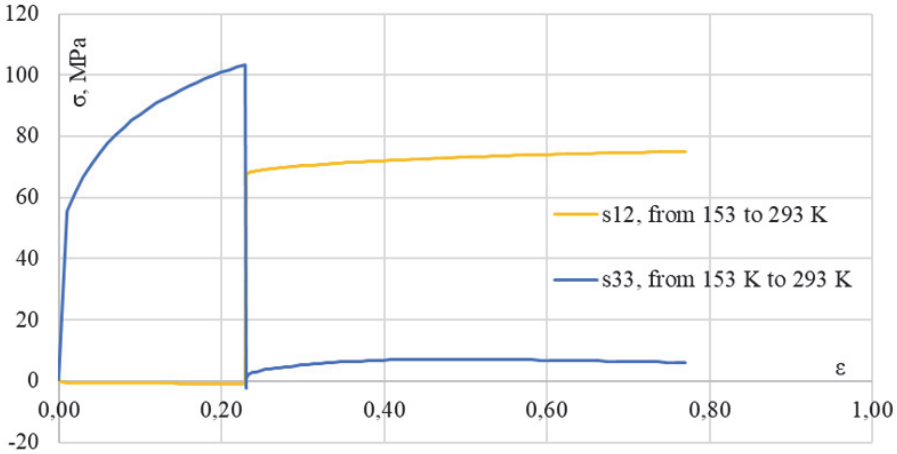

Figure 8: Dependence of stress components on the intensity of accumulated strain obtained in model calculations during rapid heating from 153 K to 293 K. The legend uses the following notations: s33 is component of stress tensor σ_{33}, s12 is component of stress tensor σ_{12}.

It can be seen that the loading temperature variations significantly affect the evolution of the stress tensor components. As in the case of monotonic loading, an increase in temperature leads to enhanced annihilation processes, which is manifested in the loading diagram as the formation of extensive regions with weak hardening. Conversely, a decrease in temperature results in pronounced hardening in the region after the strain-path change, which, in general, is not typical for orthogonal loading at a constant temperature (Fig. 5).

Conclusions

This work made it possible to test the previously proposed model [14] of inelastic deformation of FCC polycrystals under variable temperature conditions for cases of complex and reverse loadings. An extension of the model was proposed to account for enhanced annihilation under reverse loading. The behavior of a representative volume of aluminum was investigated. The model correctly describes features such as the Bauschinger effect and the formation of a *plateau* in the region after the transition to reverse loading. The calculated loading diagrams for simple shear, reverse shear, and orthogonal loading (sequential quasi-uniaxial tension and simple shear) satisfactorily agree with the experimental data [9]. In this case, the relative deviation of the numerical solution from the experimental data, defined according (8), is less than 2.8% for monotonic loading with a constant temperature, less than 2.9% for monotonic loading with a changing temperature, and no more than 7% for reversive loading.

Acknowledgements

The study was carried out with a financial support from the Ministry of Education and Science of the Russian Federation as part of the state task in the laboratory of multilevel structural and functional materials modeling, project no. FSNM-2024-0002.

References

[1] Gronostajski, Z., Pater, Z., Madej, L., Gontarz, A., Lisiecki, L., Łukaszek-Sołek, A., Łuksza, J., Mróz, S., Muskalski, Z., Muzykiewicz, W., Pietrzyk, M., Śliwa, R.E., Tomczak, J., Wiewiórowska, S., Winiarski, G., Zasadziński, J. and Ziółkiewicz S. (2019). Recent development trends in metal forming, Archives of Civil and Mechanical Engineering, 19(3), pp. 898–941. DOI: https://doi.org/10.1016/j.acme.2019.04.005

[2] Edalati, K., Bachmaier, A., Beloshenko, V.A., Beygelzimer, Y., Blank, V.D., Botta, W.J., … Zhu, X. (2022). Nanomaterials by severe plastic deformation: review of historical developments and recent advances, Materials Research Letters, 10(4), pp. 163–256. DOI: https://doi.org/10.1080/21663831.2022.2029779.

[3] Shi, B., Yanga, C., Penga, Y., Zhangb, F. and Pan F. (2022). Anisotropy of wrought magnesium alloys: A focused overview, Journal of Magnesium and Alloys, 10(6), pp. 1476–1510. DOI: https://doi.org/10.1016/j.jma.2022.03.006.

[4] Mánik, T., Holmedal, B. and Hopperstad O.S. (2015). Strain-path change induced transients in flow stress, work hardening and r-values in aluminum, Int. J. Plast., 69, pp. 1–20. DOI: https://doi.org/10.1016/j.ijplas.2015.01.004.

[5] Langi, V., Soares, G.C., Ahmed, S., Peura, P and Hokka, M. (2023). Effects of strain rate and adiabatic heating on mechanical behavior of medium manganese Q&P steels, Materials Science and Engineering: A, 865, pp. 144659. DOI: https://doi.org/10.1016/j.msea.2023.144659.

[6] Kareem, S.A., Anaele, J.U., Aikulola, E.O., Olanrewaju, O.F., Omiyale, B.O., Falana, S., Oke, S.R. and Bodunrin M.O. (2025). Hot deformation behavior of aluminum alloys: A comprehensive review on deformation mechanism, processing maps analysis and constitutive model description, Materials Today Communications, 44, pp. 112004. DOI: https://doi.org/10.1016/j.mtcomm.2025.112004.

[7] Li, Y., Zhang, H. and Li, S. (2025). Thermo-mechanical-metallurgical and damage modeling for hot stamping and warm-cutting of boron steel, Journal of Materials Research and Technology, 36, pp. 1625-1644. DOI: https://doi.org/10.1016/j.jmrt.2025.03.206.

[8] Yi, L., Li, X., Li, Y., Yu, G., Tang, Z. and Gu, Z. (2021). Investigation of the two-stage SPF process of aluminum alloy door frames, Journal of Materials Research and Technology, 15, pp. 2873-2882. DOI: 10.1016/j.jmrt.2021.09.110.

[9] Vincze, G., Rauch, E.F., Gracio, J.J., Barlat, F. and Lopes, A.B. (2005). A comparison of the mechanical behaviour of an AA1050 and a low carbon steel deformed upon strain reversal, Acta Mater., 53(4), pp. 1005-1013. DOI: https://doi.org/10.1016/j.actamat.2004.10.046.

[10] Holmedal, B. (2019). Bauschinger effect modelled by yield surface distortions, Int. J. Plast., 123, pp. 86-100. DOI: https://doi.org/10.1016/j.ijplas.2019.07.009.

[11] Yoshida, K. (2024). Crystal plasticity model for describing the work hardening of A5052-O sheets subjected to various loading paths, International Journal of Solids and Structures, 291, pp. 112697. DOI: https://doi.org/10.1016/j.ijsolstr.2024.112697.

[12] Trusov, P.V., Shveykin, A.I., Kondratyev, N.S. and Yants, A.Yu. (2021). Multilevel models in physical mesomechanics of metals and alloys: results and prospects, Physical Mesomechanics, 24(4), pp. 391-417. DOI: https://doi.org/10.1134/S1029959921040056.
[13] Shveykin, A., Romanov, K. and Trusov, P. (2022). Some issues with statistical crystal plasticity models: description of the effects triggered in FCC crystals by loading with strain-path changes, Materials, 15(19), pp. 6586. DOI: https://doi.org/10.3390/ ma15196586.
[14] Shveykin, A.I., Vshivkova, A.A. and Trusov, P.V. (2024). Two-level constitutive model of metal with a comprehensive account of temperature and strain rate changes, Physical Mesomechanics, 27(4), pp. 370-386. DOI: https://doi.org/10.1134/S1029959924040027.
[15] Shveykin, A.I., Vshivkova, A.A. and Trusov, P.V. (2024). Methods of accounting for temperature and strain rate variation in multilevel constitutive models of metal deformation (analytical review), Physical Mesomechanics, 27(2), pp. 133-151. DOI: https://doi.org/10.1134/S1029959924020036.
[16] Van Houtte, P., Li, S., Seefeldt, M. and Delannay, L. (2005). Deformation Texture Prediction: From the Taylor Model to the Advanced Lamel Model, Int. J. Plast., 21, 589-624. DOI: https://doi.org/10.1016/j.ijplas.2004.04.011.
[17] Trusov, P.V., Sharifullina, E.R. and Shveykin, A.I. (2019). Multilevel model for the description of plastic and superplastic deformation of polycristalline materials, Physical Mesomechanics, 22(5), pp. 402-419. DOI: https://doi.org/10.1134/S1029959919050072.
[18] Terentyev, D., Xiao, X., Dubinko, A., Bakaeva, A. and Duan H. (2015). Dislocation-mediated strain hardening in tungsten: Thermo-mechanical plasticity theory and experimental validation, J Mech Phys Solids, 85, pp. 1-15. DOI: https://doi.org/10.1016/j.jmps.2015.08.015.
[19] Anand, L. (2004). Single-crystal elasto-viscoplasticity: application to texture evolution in polycrystalline metals at large strains, Comput Methods Appl Mech Eng., pp. 5359-5383. DOI: https://doi.org/10.1016/j.cma.2003.12.068.
[20] Rauch, E.F., Gracio, J.J. and Barlat, F. (2007). Work-hardening model for polycrystalline metals under strain reversal at large strains, Acta Mater., 55, pp. 2939-2948. DOI: https://doi.org/10.1016/j.actamat.2007.01.003.
[21] Eghtesad, A. and Knezevic, M. (2021). Modeling cyclic plasticity of additively manufactured alloy Mar-M-509 using a high-performance spectral-based micromechanical model, Applications in Engineering Science, 7, pp. 100065. DOI: https://doi.org/10.1016/j.apples.2021.100065.
[22] Beyerlein, I.J. and Tome, C.N. (2007). Modeling transients in the mechanical response of copper due to strain path changes, Int. J. Plast., 23, pp. 640-664. DOI: https://doi.org/10.1016/j.ijplas.2006.08.001
[23] Beyerlein, I.J. and Tome, C.N. (2008). A dislocation-based constitutive law for pure Zr including temperature effects, Int. J. Plast., 24, pp. 867-895. DOI: https://doi.org/10.1016/j.ijplas.2007.07.017.
[24] Kocks, U. F., Canova, G. R. and Jonas, J. J. (1983). Yield vectors in F.C.C. crystals, Acta metall., 31(8), pp. 1243-12521. DOI: https://doi.org/10.1016/0001-6160(83)90186-4
[25] Kobaissy, A. A.-H., Ayoub, G., Nasim, W., Malik, J., Karaman, I. and Shehadeh, M. (2020). Modeling of the ECAP induced strain hardening behavior in FCC metals, Metallurgical and Materials Transactions A, 51, pp. 5453-5474. DOI: https://doi.org/10.1007/s11661-020-05971-2.